EPR, NMR, and Electrochemical Studies of Surface-Modified Carbon Microbeads

Ricardo Alcántara,* Gregorio F. Ortiz, Pedro Lavela, and José L. Tirado

Laboratorio de Química Inorgánica, Universidad de Córdoba, Edificio C3, Campus de Rabanales, 14071 Córdoba, Spain

Radostina Stoyanova and Ekaterina Zhecheva

Institute of General and Inorganic Chemistry, Bulgarian Academy of Sciences, 1113 Sofia, Bulgaria

Received January 10, 2006. Revised Manuscript Received March 2, 2006

Nongraphitic carbon microbeads were prepared by hydrothermal treatment of a glucose aqueous solution at 180 °C. Impregnation of glucose-derived carbon microbeads with citric acid was used to control the microbeads' surface and electrochemical properties. The microspherical sample thus obtained exhibited a highly disordered nanocrystalline structure and a low BET surface area. The electrochemical performance of carbon microbeads was evaluated from discharge/charge experiments in lithium and sodium cells, as well as from electrochemical impedance spectroscopy measurements. The intercalation of Li and Na in surface-modified carbon microbeads was explored by EPR and NMR spectroscopy. It was shown that similar mechanisms operate for lithium and sodium insertion into disordered carbons. The observed Curie-like behavior and the change in intensity of the EPR signals as a function of cell voltage agreed well with lithium insertion into different sites of disordered carbon structures forming paramagnetic centers. Microspherical carbon samples with high reversible capacities in both Li and Na cells commonly exhibit low concentrations of paramagnetic centers.

1. Introduction

Carbonaceous materials are widely used as negative electrodes in lithium-ion batteries.[1,2] The first commercial lithium-ion batteries used soft carbons obtained at about 1200 °C. In a second generation of lithium-ion batteries, hard carbons were employed. One advantage of disordered carbon electrodes as compared with graphite electrodes is that the former suffer little volume change upon lithium insertion. Actually, lithium-ion batteries with negative electrodes comprising a mixture of carbon and metal have started to be commercialized. However, the study and optimization of carbonaceous materials still remains an important point in developing new high-performance batteries.

Microspherical carbon particles offer several advantages in their use as electrodes, such as an easy preparation without a preferred particle orientation.[3−5] Thus, to improve the electrochemical performance of natural graphite, Yoshio et al. have obtained graphite flakes rolled into spheres.[3] Graphitizable mesocarbon microbeads obtained from petroleum pitch also display a good performance.[4,5] On the other hand, nongraphitizable hard carbons can reach reversible capacities higher than the maximum theoretical capacity for graphite (372 mA h g^{-1}).[6,7] Sugar is a typical precursor for nongraphitizable carbon materials, although structural control of the resulting product is difficult.[8] Hard carbon microbeads can be prepared by hydrothermal treatment of an aqueous glucose solution (polycondensation reaction) followed by heating it under an inert atmosphere (carbonization process).[9,10] A different procedure for obtaining a special type of hard carbon microbeads, which has potential applications in supercapacitors and batteries, is from a resorcinol/formaldehyde mixture that first yields an aquagel and finally a carbon xerogel.[11,12] Because hard carbons obtained from resorcinol (or from glucose) exhibit porous systems that may be controlled on the nanoscopic level by changing the synthesis conditions, these materials can be considered to be nanocarbons.[13] Large external surface areas can be deleterious for lithium-ion battery electrodes, because of electrolyte decomposition and irreversible reactions that can occur on the electrode surface. Thus, Béguin et al. have recently found a relationship between the irreversible capacity

* To whom correspondence should be addressed. Phone: 34 95721 8637. Fax: 34 95721 8621. E-mail: iq2alror@uco.es.

(1) Nishi, Y. *Chem. Rec.* **2001**, *1*, 406.
(2) Winter, M.; Besenhard, J. O.; Spahr, M. E.; Novák, P. *Adv. Mater.* **1998**, *10*, 425.
(3) Yoshio, M.; Wang, H.; Fukuda, K.; Umeno, T.; Abe, T.; Ogumi, Z. *J. Mater. Chem.* **2004**, *14*, 1754.
(4) Marsh, H.; Martínez-Escandell, M.; Rodríguez-Reinoso, F. *Carbon* **1999**, *37*, 363.
(5) Alcántara, R.; Fernández-Madrigal, F. J.; Lavela, P.; Tirado, J. L.; Jiménez-Mateos, J. M.; Gómez de Salazar, C.; Stoyanova, R.; Zhecheva, E. *Carbon* **2000**, *38*, 1031.
(6) Dahn, J. R.; Zheng, T.; Liu, Y. H.; Xue, J. S. *Science* **1995**, *270*, 590.
(7) Peled, E.; Eshkenazi, V.; Rosenberg, Y. *J. Power Sources* **1998**, *76*, 153.
(8) Xing, W.; Xue, J. S.; Dahn, J. R. *J. Electrochem. Soc.* **1996**, *143*, 3046.
(9) Wang, Q.; Li, H.; Chen, L.; Huang, X. *Solid State Ionics* **2002**, *152*, 43.
(10) Wang, Q.; Li, H.; Chen, L.; Huang, X. *Carbon* **2001**, *39*, 2211.
(11) Pekala, R. W. *J. Mater. Sci.* **1989**, *24*, 322.
(12) Alcántara, R.; Lavela, P.; Ortiz, G. F.; Tirado, J. L. *Electrochem. Solid State Lett.* **2005**, *8*, A222.
(13) Inagaki, M.; Kaneko, K.; Nishizawa, T. *Carbon* **2004**, *42*, 1401.

10.1021/cm060060p CCC: $33.50
Published on Web 03/29/2006

and the active surface area of carbons.[14] Other preparation methods for spherical carbons are based on the use of phenolic resins and silica powder[15] and on oligophenylene precursors.[16]

The complex electrochemical behavior in lithium test cells of hard carbons obtained from sugar depends on many factors.[8] Several models have been proposed in the literature for explaining the intercalation of lithium into nongraphitic carbon materials.[17−22] Thus, the large capacities observed for nongraphitic carbons have been proposed to result from the formation of Li_2 covalent molecules,[19] multilayer lithium on the graphene surface,[21] and Li−C−H bonds.[22] The high capacity of mesocarbon microbeads was explained on the basis of lithium incorporation in carbon cavities.[18,23] For hard carbons, the most widely accepted model is the house of cards model proposed by Dahn and co-workers.[24] In this model, the extra capacity is ascribed to lithium adsorption on the internal surfaces of single graphene layers. Nanopores are incorporated between the graphene layers, which are arranged like a house of cards. Hard carbons usually show complicated voltage profiles of charge and discharge that indicate different types of insertion processes.[20] In addition to the pure soft and hard carbons concepts, we must point out that carbonaceous samples with intermediate characteristics between these two extremes are quite usual, and then the interpretation of their properties is even further complex.

The aim of this work is to prepare nongraphitic carbon spherical particles and to study their electrochemical behavior in lithium and sodium test cells. The target materials are carbons with internal porosity that can be filled with alkali metal near 0 V, together with low external surface area to minimize the irreversible reactions with the electrolyte solution. To control the surface and textural properties, and as a way to improve the electrochemical behavior, we have treated the microspherical hard carbon particles with citric acid. The intercalation mechanism is explored by EPR and NMR.

2. Experimental Section

To obtain carbon microbeads, we used an optimized preparation method in which the addition of citric acid was used to obtain samples with low specific surface areas. A 3 M glucose solution in water was hydrothermally treated at 180 °C for 48 h. After hydrothermal treatment, the precursor was added into a 0.14 M citric acid ($C_6H_8O_7 \cdot H_2O$ from Panreac) solution in water; it was then stirred for 14 h, filtered, and finally annealed at 850 °C for 1 h under an Ar flow (50 mL/min). The furnace was heated from room temperature to the desired annealing temperature for 3 h and then cooled to room temperature by switching off the power. The final yield of the total process was about 50 wt %. In addition, several samples were obtained at 800, 950, and 1020 °C.

X-ray diffraction (XRD) experiments were carried out in a Siemens D5000 instrument equipped with Cu Kα radiation, and scans with 0.02° 2θ and 6 s steps were used. Scanning electron microscopy (SEM) images were recorded on a JEOL JSM6300 instrument. The elemental composition (carbon and hydrogen content) was analyzed on a Eurovector-EA3010 instrument. The surface areas of previously degassed carbon samples were measured by using N_2 physical adsorption (Brunauer−Emmett−Teller, BET method) in a Micromeritics apparatus.

The electrochemical discharge/charge experiments were performed in an Arbin instrument (College Station, TX), working at *C*/*n* rate. This means that one mole of alkali metal reacts with one mole of C_6 in *n* hours. Voltage limits were 0.003 and 2.0 V vs Li^+/Li. Swagelok type cells with plastic bodies were employed with a lithium disk as counter electrode and a carbon-based (92% active material and 8% PVDF as binder) working electrode. The electrolyte was 1 M $LiPF_6$ in EC:DEC (1:1 w/w) supported in Whatmann glass microfibers. The active material−binder mixture dispersed in *n*-methyl pyrrolidone was deposited on a Cu foil (Goodfellow). Prior to electrochemical measurements, all working electrodes were dried at 120 °C under a dynamic vacuum for several hours. The test cells were mounted in a glovebox under an Ar atmosphere. For sodium test cells, we used $NaClO_4$ 1 M in EC:DMC as the electrolyte and Na metal as the counter electrode.

Electrochemical impedance spectroscopy (EIS) measurements were carried out in an Autolab instrument using three-electrode cells. Reference and counter electrodes were Li disks, whereas the working electrode was about 1.7 mg of carbon supported on a Cu foil with a 9 mm diameter. Spectra were recorded after discharge to 0.00 V at a *C*/50 rate and a relaxation period. Multiplying by the electrode active mass normalized the impedance values, and the spectra were represented in Ω g units.

Electron paramagnetic resonance (EPR) spectra were registered at the X-band (9.23 GHz) as the first derivative of the absorption signal using an ERS 220/Q spectrometer in the temperature range 90−410 K. The measurements were made on about 10 mg of powdered samples in quartz tubes, which do not contain ferric impurities. Microwave power was varied between 1 and 5 mW, and the modulation amplitude was 0.2 mT. The *g* factors were established with respect to a Mn^{2+}/ZnS standard. The signal intensity was determined by double integration of the experimental EPR spectrum. The absolute spin concentration was calculated on the basis of DPPH and Mn^{2+}/ZnS as standards. For EPR measurements of anode materials, we manipulated the samples in a glovebox in an Ar atmosphere.

^{7}Li magic angle spinning nuclear magnetic resonance (MAS NMR) spectra were recorded on a Bruker Avance 400 instrument, working at a 14 kHz spin rate. The reference was LiCl 1 M in water (0 ppm). Electrodes were washed with propylene carbonate before NMR measurements.

3. Results and Discussion

3.1. Microstructure, Texture, and Surface. As a result of the hydrothermal treatment at 180 °C, glucose molecules were polymerized into carbonaceous particles with well-defined spherical morphologies. Residual water contents were difficult to eliminate even by heating the products to 200 °C under a vacuum for several days. Thus, the instability of

(14) Béguin, F.; Chevallier, F.; Vix-Guterl, C.; Saadallah, S.; Bertagna, V.; Rouzaud, J. N.; Frackowiak, E. *Carbon* **2005**, *43*, 2160.
(15) Kwon, O. J.; Jung, Y. S.; Kim, J. H.; Oh, S. M. *J. Power Sources* **2004**, *125*, 221.
(16) Bonino, F.; Brutti, S.; Reale, P.; Scrosati, B.; Gherghel, L.; Wu, J.; Müllen, K. *Adv. Mater.* **2005**, *17*, 743.
(17) Zheng, T.; Xue, J. S.; Dahn, J. R. *Chem. Mater.* **1996**, *8*, 389.
(18) Mabuchi, A.; Tokumitsu, K.; Fujimoto, H.; Kasuh, T. *J. Electrochem. Soc.* **1995**, *142*, 1041.
(19) Sato, K.; Noguchi, M.; Demachi, A.; Oki, N.; Endo, M. *Science* **1994**, *264*, 556.
(20) Mochida, I.; Ku, C. H.; Korai, Y. *Carbon* **2001**, *39*, 399.
(21) Yazami, R.; Deschamps, M. *J. Power Sources* **1995**, *54*, 411.
(22) Dahn, J. R.; Zheng, T.; Liu, Y.; Xue, J. S. *Science* **1995**, *270*, 590.
(23) Tokumitsu, K.; Fujimoto, H.; Mabuchi, A.; Kasuh, T. *Carbon* **1999**, *37* (7), 1599.
(24) Liu, Y.; Xue, J. S.; Zheng, T.; Dahn, J. R. *Carbon* **1996**, *34*, 193.

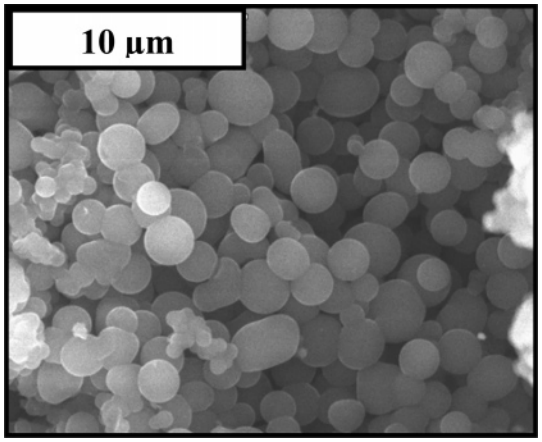

Figure 1. SEM image of carbon microbeads.

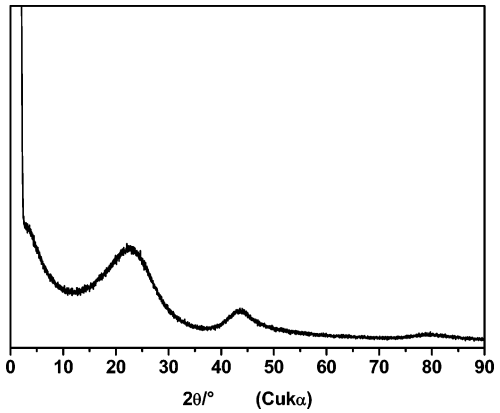

Figure 2. XRD pattern of carbon microbeads.

the particles to the electron beam made it difficult to obtain electron microscopy images of sufficient quality. After being annealed in an Ar flow at 850 °C, the carbon particles maintained a perfect spherical shape with diameters of about 3 μm (Figure 1).

The XRD pattern of a carbon microbead sample is shown in Figure 2. The XRD patterns exhibit a highly broadened (002) Bragg reflection of graphite near 23° 2θ, which is typical of nongraphitic carbon materials with highly disordered nanocrystalline structures. Crystallite size calculated by the Scherrer method in the *c*-axis direction (Lc) was 10 Å. It is known that lithium-insertion capacities surpassing the theoretical capacity of the graphite electrode are observed only when carbons with very small crystallite sizes are used. The experimental (002) peak-to-background ratio (*R* parameter), which is proportional to the number of parallel-stacked graphene layers, takes a value of 2.2. Dahn et al. suggested that the best microporous carbons for lithium batteries have low values of this empirical *R* parameter.[25] The increase in intensity at low angles (below ca. 12° 2θ) results in a kind of tail that is characteristic of porous carbons, in which the cavities are X-ray scatter centers.[26] The broad and low-intensity peak at about 5° 2θ results from the packing of the structural units with an average nearest neighbor center-to-center distance of about 2 nm.[23] The packing of the structural units is important for lithium accommodation.

Table 1. Properties of Carbon Microbead Samples Obtained at 850 °C with Citric Acid (lines 1 to 3) and without Citric Acid (lower line)

BET area ($m^2\ g^{-1}$)	H/C (%)	rev. cap. vs Li[a] (mA h g^{-1})	irrev. cap. vs Li[a] (mA h g^{-1})	rev. cap. vs Na[b] (mA h g^{-1})
3	0.81	381 (*C*/5)	181 (*C*/5)	277
3	0.81	506 (*C*/20)	149 (*C*/20)	277
3	0.81	550 (*C*/50)	162 (*C*/50)	277
2	0.94	442 (*C*/20)	166 (*C*/20)	246

[a] Reversible and irreversible capacities are given at several *C*/*n* rates. This means that in *n* hours, 1 mole of alkali metal reacts with one C_6 mole. [b] Capacities are given at a *C*/80 rate.

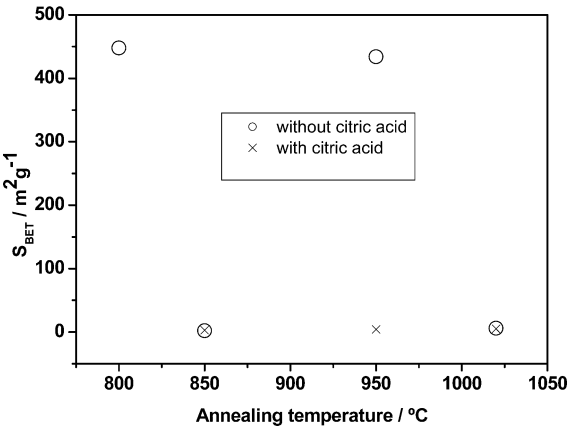

Figure 3. BET surface area for carbon microbeads obtained with or without citric acid treatment.

The sample has a significant hydrogen content (Table 1), which comes from the precursor organic molecules. The presence of hydrogen can influence on the electrochemical reaction of low-temperature carbons with lithium,[6,27] as will be discussed below.

The experimental BET surface area of the obtained carbon microbeads sample is 3 m^2/g (Table 1). Microporosity accessible to N_2 molecules was not detected. Larger and fluctuating surface area values are obtained for carbon microbead samples obtained from the hydrothermal treatment of glucose without treatment with citric acid and with annealing between 800 and 1020 °C (Figure 3). When the heating temperature is below about 1000 °C, carbons are made of mosaic domains formed by stacks of parallel layers.[28] Because the direction of the preferred orientation plane changes randomly from one domain to another, it results in a porous texture with irregularly shaped pores. In low-temperature (soft and hard) carbons, pore walls have a zigzag structure. Pore size differs greatly when soft or hard carbons are considered. In soft carbons, each cluster of parallel-oriented layers extends in a long range, which is larger than a few micrometers, whereas the average pore size is less than 100 Å in hard carbons.[28] The control of porosity in hard carbons is a difficult task. Marked changes in surface area are frequently related to complex phenomena of pore-closure processes and cross-linking between graphene layers, which are difficult to control and are highly influenced by subtle variations in the synthesis conditions. Small BET surface area values do not necessarily indicate the absence

(25) Dahn, J. R.; Xing, W.; Gao, Y. *Carbon* **1997**, *35*, 825.
(26) Gibaud, A.; Xue, J. S.; Dahn, J. R. *Carbon* **1996**, *34*, 499.
(27) Papanek, P.; Radosavljevic, M.; Fischer, J. E. *Chem. Mater.* **1996**, *8*, 1519.
(28) De Fonton, S.; Oberlin, A.; Inagaki, M. *J. Mater. Sci.* **1980**, *15*, 909.

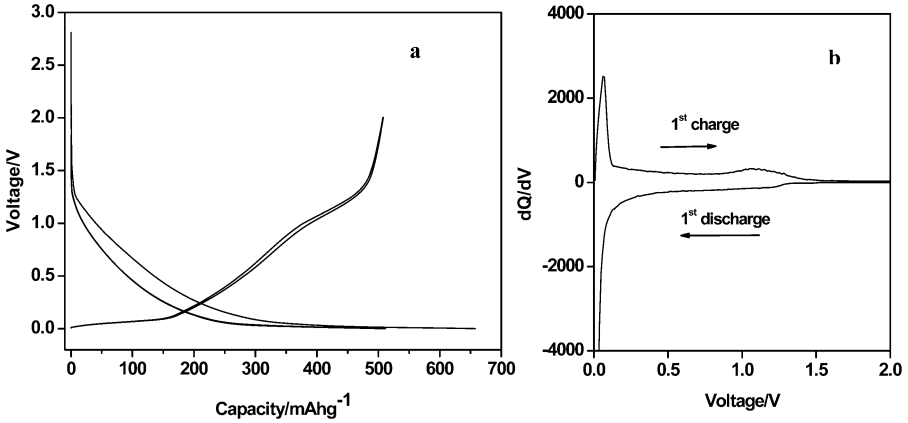

Figure 4. (a) Voltage−capacity curves of the first cycles in Li cells of carbon microbeads obtained from glucose. (b) Detailed view of the derivative curves corresponding to the first discharge/charge cycle. Rate = *C*/20.

of internal voids, such as closed pores, that are not accessible to N_2 but that may remain accessible to lithium. Closed micropores have certain similarities with some forms of nanocarbons such as fullerenes.[29] In fact, fullerenes have been considered to be an idealized model of nanopores in carbon materials.[30] Thus, the presence of sp^3 like bonds introduces curvature into the sp^2-bonded graphitic planes.[31] In our samples, it can be considered that citric acid molecules are first deposited on the surface of the previously obtained carbon microbeads and then thermally decomposed into carbon, thus closing the open pores originally present on the surface of carbon microbeads. In addition, the acidic groups from citric molecules may react with the residual hydroxyl groups that still remain in the carbon microbeads after the hydrothermal treatment and act as cross-linking modifiers.

It is expected that the carbon coating should have notable consequences on the electrochemical behavior. Surface modification of graphite by carbon coating has been previously reported in the literature.[32] Yoshio et al.[33] coated hard carbon beads with soft carbon using thermal vapor decomposition. Pyrocarbon coating on hard carbon has been recently reported, and a reduction of irreversible capacity and an improvement of the cyclability were shown.[34] As compared with other methods of carbon coating, such as chemical vapor deposition from hydrocarbons, impregnation with citric acid in aqueous media is easier and cheaper with a good control of surface properties.

3.2. Electrochemistry. The voltage vs specific capacity curves of lithium test cells using carbon microbead electrodes are shown in Figure 4. The irreversible capacity observed at 2 V after the first discharge/charge cycle and the reversible capacities in the second discharge between 2 and 0 V are shown in Table 1. The derivative curves are also shown in Figure 4. Each peak in the derivative curve corresponds to a nearly constant voltage region (or plateau) in the voltage−capacity curve.

The voltage−capacity curves and the corresponding derivative curves are typical of nongraphitic carbons. The characteristic stages of graphite intercalation compounds were not observed. Several main regions can be resolved in Figure 4. According to previous literature,[2,35] irreversible reactions and formation of a passivating surface film on graphite can occur in the 1.2−0.8 V region. During the first discharge (Li intercalation), a voltage plateau is not observed at about 1.2−0.8 V in Figure 4. Between ca. 0.2 and 0.8 V, a sloped voltage−capacity region can be discerned, which is characteristic of lithium extraction/insertion processes between disorderly stacked graphene layers. Finally, the most-intense signal is located near 0 V, which is characteristic of hard carbons and is ascribable to lithium adsorption on pore surfaces.[6] The fourth main feature is a signal in the derivative curve located between about 0.9 and 1.4 V, which is ascribed to lithium in the border of graphene layers[36] and/or in the vicinity of hydrogen−carbon bonds.[6] This signal, located at about 0.9−1.4 V in the charge process (Li deintercalation), is not observed in the discharge. In contrast, the main signal at 0 V is more intense in the discharge than in the charge process. This behavior leads to hysteresis loops in the voltage curve that is typical of low-temperature carbons containing residual hydrogen and that is associated with capacity fade on prolonged discharge−charge cycling.[6] The location of the residual hydrogen is not completely known, but it is expected that hydrogen atoms preferentially saturate the carbon valences on the perimeter of the aromatic layers;[27] however, hydrogen in other environments of hard carbons cannot be discounted.[37] The insertion of lithium near the H sites involves changes in the nature of the bonding in the carbon network. Recent computational simulations have shown that the flexibility and variance of pore diameters for lithium uptake are affected by the hydrogen and carbon relative content.[30] The C−H and C−C bonds with sp^3 hybridization are more flexible than planar C═C bonds with

(29) Buiel, E.; George, A. E.; Dahn, J. R. *J. Electrochem. Soc.* **1998**, *145*, 2252.
(30) Nicolau, D. V. *Nanotechnology* **2005**, *16*, 488.
(31) Amaratunga, G. A. J.; Chowalla, M.; Kiely, C. J.; Alexandrou, I.; Aharonov, R.; Devenish, R. M. *Nature* **1996**, 383, 321.
(32) Yoon, S.; Kim, H.; Oh, S. M. *J. Power Sources* **2001**, *94*, 68.
(33) Yoshio, M.; Wang, H.; Fukuda, K.; Abe, T.; Ogumi, Z. *Chem. Lett.* **2003**, *32*, 1130.
(34) Ohzawa, Y.; Yamanaka, Y.; Naga, K.; Nakajima, T. *J. Power Sources* **2005**, *146*, 125.
(35) Fong, R.; Sacken, U. V.; Dahn, J. R. *J. Electrochem. Soc.* **1990**, *137*, 2009.
(36) Matsumura, Y.; Wang, S.; Mondori, J. *Carbon* **1995**, *33*, 1457.
(37) Honeybone, P. J. R.; Newport, R. J.; Walters, J K.; Howells, W. S.; Tomkinson, J. *Phys. Rev. B* **1994**, *50*, 839.

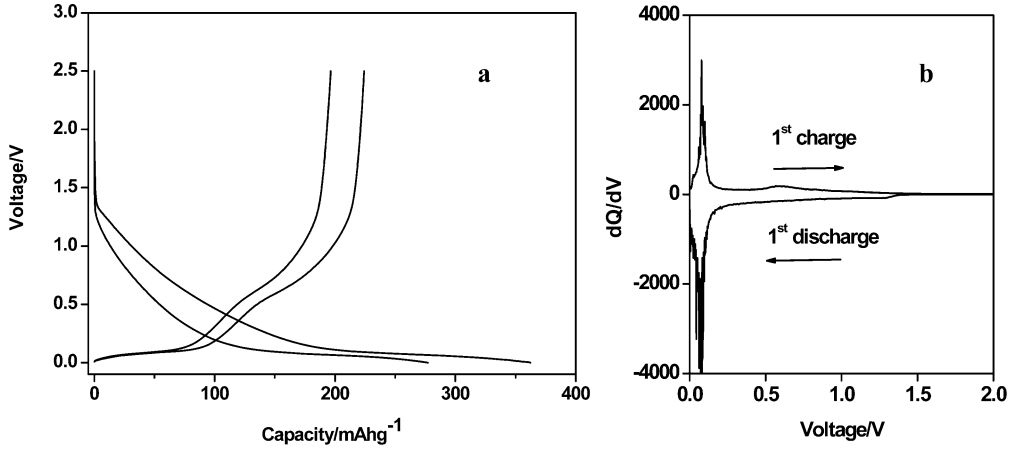

Figure 5. (a) Voltage−capacity curves of the first cycles in Na cells of carbon microbeads. (b) Derivative curves of the first discharge/charge cycle. Rate = *C*/80.

sp^2 hybridization in nonhydrogenated structures. The sp^3-hybridized carbons allow for the formation of inner cavities with reduced sphericity, whereas the aromatic planar sp^2-hybridized structures give rigidity to the total system and the ability to support the swelling induced by lithium insertion. Unfortunately, the decrease in hydrogen content with an increase in annealing temperature can yield pore closure and a decrease in the initial reversible lithium capacity, which is associated with the filling of the pores.[29]

Large external surface areas enhance the irreversible reactions between inserted lithium and the liquid electrolyte and decrease the efficiency of the first discharge/charge cycle.[38] Thus, pore closure plays an important role.[39] A reason for the reduction of the 0 V region capacity is the increase in the chemical potential of lithium that is inserted within the pores in which the radius is large.[39] To obtain good electrochemical behavior in this type of materials, we must avoid large surface areas to decrease the extension of irreversible processes. In contrast, internal nanocavities and voids, which may be inaccessible to N_2 molecules, are needed to yield large reversible capacities in the 0 V region. The influence of micropore structure on Li capacity in hard carbon beads at different current densities has been studied by Hu et al.[40] Smaller micropores showed larger capacities at high current density.

To optimize the electrochemical behavior, it is very important to first optimize the synthesis conditions. For this reason, we have studied the treatment with citric acid of carbon microbeads previously obtained from the hydrothermal treatment of glucose. Although, according to the BET surface results, the treatment with citric acid has closed the pores that are accessible to N_2 molecules, the occurrence of an intense 0 V region is indicative of internal voids remaining accessible to accommodate lithium (and sodium). The selected sample was obtained from glucose followed by hydrothermal treatment, the addition of 0.14 M citric acid solution, and finally annealing at 850 °C. The sample exhibited a reversible specific capacity of about 500 mA h g^{-1} between 1.5 and 0.0 V (Table 1). The observed capacity depends on the kinetic conditions used in the experiment. Larger capacities are obtained for slower kinetics. At very low rate (*C*/50), a reversible capacity of 550 mA h g^{-1} is achieved. The treatment with citric acid is shown to be an excellent method for improving the electrochemical performance of carbon microbeads obtained from glucose. However, to achieve high specific capacities at very high rates, we need small particle sizes.[41] Yoshio et al. previously reported carbon-coated hard carbon beads, obtained through thermal vapor decomposition of benzene, with enlarged reversible capacities. The improvement of the reversible capacity was ascribed to the increase in the electric conductivity.[33]

The electrochemical behavior has also been studied in sodium test cells (Figure 5). Sodium could be an alternative to lithium batteries. It was previously reported that the Na and Li reversible capacity of nongraphitic soft carbons decreases with increased preparation temperatures, between 600 and 1200 °C.[42] For annealing temperatures higher than about 1200 °C, when graphitization starts, the Li capacity increases whereas the Na capacity remains very low.[42] The capacity of graphitized carbon to electrochemically insert Na in the interlayer space is low, but increases when the graphitic carbon is ball milled.[43] The insertion of sodium in disordered carbons, such as cokes[42] and carbon blacks,[44] takes place through a sloped voltage curve. By contrast, the insertion of sodium into nongraphitizable hard carbons takes place mainly through an extended plateau near 0 V.[45] As with Li insertion, this is indicative of the ability of different sites in carbons for Na insertion. The voltage−capacity and derivative curves are quite similar in Figures 4 and 5. It is worth noting that the signal at 0.9−1.4 V of the charge process in lithium cells is also observed in sodium test cells, although with a lower intensity between about 0.4 and 0.9 V. These features

(38) Chevalier, F.; Gautier, S.; Salvetat, J. P.; Clinard, C.; Frackowiak, E.; Rouzard, J. N.; Béguin, F. *J. Power Sources* **2001**, *97*−*98*, 143.
(39) Buiel, E.; Dahn, J. R. *Electrochim. Acta* **1999**, *45*, 121.
(40) Hu, J.; Li, H.; Huang, X. *Solid State Ionics* **2005**, *176*, 1151.
(41) Wang, H.; Abe, T.; Maruyama, S.; Iriyama, Y.; Ogumi, Z. *Adv. Mater.* **2005**, *17*, 2857.
(42) Alcántara, R.; Jiménez-Mateos, J. M.; Tirado, J. L. *J. Electrochem. Soc.* **2002**, *149*, A201.
(43) Alcántara, R.; Lavela, P.; Ortiz, G. F.; Tirado, J. L.; Menéndez, R.; Santamaría, R.; Jiménez-Mateos, J. M. *Carbon* **2003**, *41*, 3003.
(44) Alcántara, R.; Jiménez-Mateos, J. M.; Lavela, P.; Tirado, J. L. *Electrochem. Commun.* **2001**, *3*, 639.
(45) Stevens, D. A.; Dahn, J. R. *J. Electrochem. Soc.* **2000**, *147*, 1271.

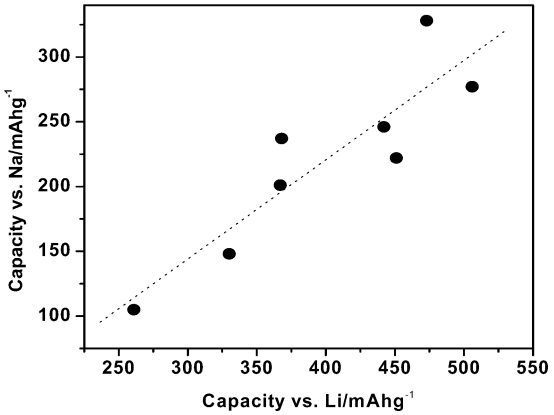

Figure 6. Specific capacity of microspherical carbon samples in sodium cells vs capacity in lithium cell. Linear fitting is shown as a dotted line.

strongly suggest the existence of similar mechanisms for sodium and lithium insertion, which is in line with previous studies.[12,45] However, the relatively lower stability of both sodium compounds and the passivating films in currently used solvents diminishes the electrochemical performance on cycling.[12] The best capacity retention in sodium cells is exhibited by the carbon microbead sample obtained by glucose and citric acid treatment and annealing at 1020 °C, which shows 250 mA h g^{-1} after 30 cycles.

Taking into account several samples prepared from the hydrothermal treatment of a glucose aqueous solution (with or without the addition of citric acid) and annealing between 800 and 1020 °C, we found a nearly linear relationship between the experimental reversible capacities in lithium and sodium cells (Figure 6). This feature supports the existence of similar mechanisms for lithium and sodium insertion into disordered carbons. These mechanisms involve alkali metal insertion between disordered stacked carbon layers, reaction with the borders of graphene layers near H-atoms and defect sites, and adsorption on the surfaces of graphene cavities.

3.3. Impedance Spectroscopy. To further study the role of interfacial films on the performance of the electrodes and the effect of citric acid treatments, we have recorded the impedance spectra of carbon microbead electrodes at 0 V vs Li^+/Li. It is known that at higher voltages, the impedance spectra are less well-defined and the separation between the different semicircles is less evident.[41] All the impedance spectra exhibit two depressed semicircles in the region of high and medium frequencies and a sloped line at low frequencies (Figure 7). The semicircles represent ion-transport resistances and interfacial capacitances. The semicircle at high frequencies is ascribed to the lithium transfer through the passivating surface film. This surface film results from the precipitation of solution ionic species, such as lithium carbonate and lithium oxide, which adhere to the carbon surface. The semicircle at medium frequencies is assigned to the charge-transfer resistance and lithium transfer toward the carbon particles. The sloped line is assigned to lithium diffusion in the carbon particle bulk (Warburg type element). The impedance spectra were fitted to the following equivalent circuit: $[R_e(R_{sl}Q_{sl})(R_{ct}W)Q_{ct}]$. The elements between brackets are arranged in parallel, and the elements between square brackets are arranged in series. R represent a resistor, Q a constant phase element and W is a Warburg

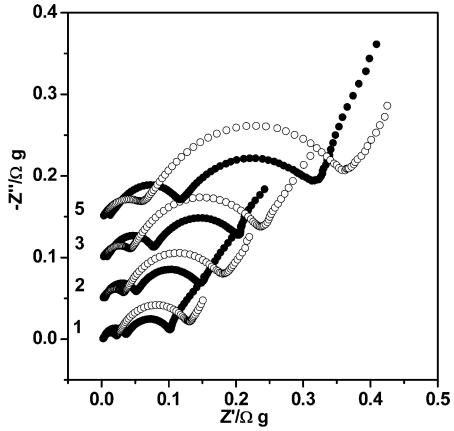

Figure 7. Impedance spectra of carbon electrodes at 0 V vs Li^+/Li for different cycle numbers (1−5). Closed symbols: carbon microbeads obtained at 850 °C. Open symbols: carbon microbeads treated with citric acid and obtained at 850 °C. Spectra have been successively shifted along the vertical axis.

Table 2. Mass-Normalized Resistances (in Ω g units) Obtained from Impedance Spectra of Carbon Microbeads at Different Cycle Numbers[a]

	microbeads from glucose only		microbeads from glucose + citric acid	
cycle	R_{sl}	R_{ct}	R_{sl}	R_{ct}
1	0.03	0.06	0.02	0.10
2	0.05	0.09	0.03	0.14
3	0.08	0.11	0.05	0.18
5	0.12	0.20	0.06	0.29

[a] R_{sl} = surface-layer resistance; R_{ct} = charge-transfer resistance.

element. The calculated surface-film resistances (R_{sl}) and charge-transfer resistances (R_{ct}) at different cycle numbers are shown in Table 2.

The impedance values tend to increase upon cycling, contributing to the capacity fade. The formation of cracks in the surface films due to swelling of the particles, which allow further reaction of the carbon electrode surface with solution species, and changes in the surface-layer thickness may contribute to the impedance rise upon cycling.[46,47] Very large volume changes upon lithium insertion that would contribute to degradation are not expected for nongraphitic carbon electrodes. However, it is known that hydrogen-containing carbon materials do not maintain their capacities for many cycles.[6] The reduction of C_{60} by lithium in the presence of aliphatic amines (H source) has been used to obtain $C_{60}H_{36}$, in which the spherical fullerene structure is distorted.[47] Keeping in mind this last feature and considering that nongraphitic carbons contain Li-filled voids when discharged at 0 V vs Li^+/Li, we may assume that the Li filling of the voids may affect the C−H bonds and the local microstructure, resulting in structural degradation on cycling, impedance rise, and capacity fade.

The derived resistance values can be compared between different samples. Thus, by comparison of carbon microbead samples that have been obtained at 850 °C, it is observed that the R_{sl} values are smaller for the sample treated with citric acid compared to the sample without citric acid.

(46) Aurbach, D. *J. Power Sources* **2000**, *89*, 206.
(47) Barsoukov, E.; Kim, J. H.; Kim, J. H.; Yoon, C. O.; Lee, H. *J. Electrochem. Soc.* **1998**, *145*, 2711.

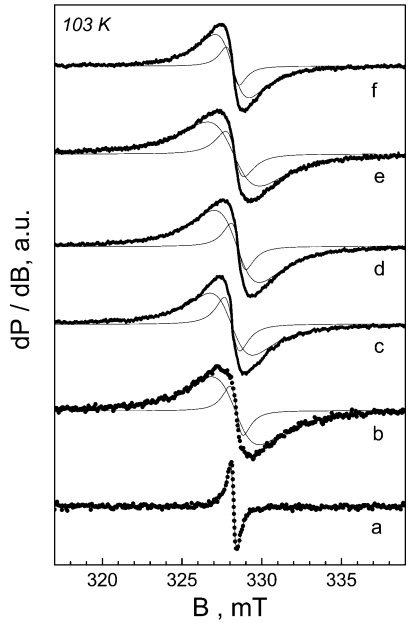

Figure 8. EPR spectra at 103 K of (a) the original carbon microbeads, (b) after the first discharge down to 0.5 and (c) 0 V vs Li, and also after discharge down to 0 V and subsequent charge up to (d) 0.6 and (e) 2 V vs Li, as well as after the first discharge down to (f) 0 V vs Na.

However, the R_{ct} values are smaller for the sample that has not been treated with citric acid. An analogous behavior was previously observed by Yoon et al. in coke-coated graphite and was explained as being due to less-severe electrolyte decomposition and a smaller electrochemically active surface area for lithium intercalation in the coated electrode.[32] Recently, Béguin et al. also observed a similar behavior.[14]

3.4. EPR. In an attempt to examine the carbon microbeads, we undertook EPR spectroscopy. EPR is a useful tool for the examination of carbonaceous materials with respect to their structural transformation during thermal treatment.[49−57] During the thermal pyrolysis of organic materials up to 1000°C, it has been shown that EPR enables one to detect the localized paramagnetic centers assigned to aromatic π radicals.[49−54] These radicals have been found to react electrochemically with Li and Na.[55−57]

Figure 8a shows the EPR spectrum of the carbon microbead sample obtained from glucose and citric acid treatment. An isotropic signal with a Lorentzian line shape, $g = 2.005$, and a line width of 0.33 ± 0.02 mT is detected. The temperature variation in the signal intensity obeys Curie-like behavior: the ratio of the signal intensity determined at 103 to that at 293 K is 2.4. The EPR parameters of the signal are consistent with localized radicals. The origin of these localized radicals can be associated with an imperfect carbon structure, such as dangling bonds with unpaired electrons in the borders of small-size graphene sheets.[58]

The EPR spectra of the carbon microbeads after the first discharge down to 0.5 and to 0 V vs Li and also after discharge down to 0 V and subsequent charge up to 0.6 and 2 V vs Li are shown in Figure 8b−e. For the sake of comparison, the first discharge down to 0 V vs Na is also shown (Figure 8f). As one can see, the signal coming from the original localized radicals disappears after the electrochemical interaction with Li and Na. The same feature was established for petroleum cokes treated below 1000 °C and ascribed to the reaction with aromatic radicals.[56] The lithium reactions with dangling bonds and hydrogen in the edge of the graphene layers, resulting in covalent C−Li bonds, can contribute to the disappearance of this signal in lithiated nongraphitized carbons.[58]

Two new signals, with different line widths, are visible in the EPR spectra regardless of whether Li or Na was used. The first signal has a line width of about 0.9 mT, whereas the line width of the second signal is about 3 mT. Both signals have nearly the same g value (about 2.005), and their intensities display Curie-like behavior between 103 and 313 K. The intensity of the broader signal is about 3 times higher than that of the narrower signal. It is important to note that the intensities of both signals are about one order of magnitude higher than that of original localized radicals. These parameters allow for the assignment of the new EPR signals to localized paramagnetic centers with different local environments. Both signals are observed in the discharged and charged electrodes and exhibit higher intensities for the electrode discharged down to 0 V and then charged to 2.0 V. It is worth remembering that the resonance signal for graphite intercalation donor compounds is usually attributed to conduction electrons in large graphene layers. Zhou et al. have ascribed the Pauli type EPR contribution to lithium insertion into ordered structures and the non-Pauli contribution to lithium insertion into disordered structures.[59] The change in EPR intensity with the state of charge for both graphite and low-temperature carbons has been previously reported.[59] When lithium intercalates into graphite, the EPR intensity continuously increases because of spin−orbit interactions between intercalated lithium and graphite crystallites. However, for disordered carbons, the insertion of lithium into cavities near 0 V and the consequent formation of lithium clusters decrease the EPR intensity. The Curie-like behavior and the change in the intensity of the EPR signals that are observed here then agree well with lithium insertion into different sites of carbon-disordered structures. One possible explanation is that one signal comes from localized paramagnetic centers formed after Li interaction with the edges of graphene layers or Li intercalation between turbostratic layers and the other from localized paramagnetic centers formed after Li adsorption on the surface of small-

(48) Zhang, J. P.; Wang, N. X.; Yang, Y. X.; Yu, A. G. *Carbon* **2004**, *42*, 667.
(49) Singer, L. S. *Proceeding of the Fifth Carbon Conference*; Pergamon Press: Oxford, U.K., 1963; Vol. II, p 37.
(50) Mrozowski, S. *Carbon* **1979**, *17*, 227.
(51) Emmerich, F. G.; Rettori, C.; Luengo, C. A. *Carbon* **1991**, *29*, 305.
(52) Delhaes, P.; Carmona, F. *Carbon* **1972**, *10*, 677.
(53) Kawamura, K. *Carbon* **1998**, *36*, 1227.
(54) Alcántara, R.; Fernández-Madrigal, F. J.; Lavela, P.; Tirado, J. L.; Jiménez Mateos, J. M.; Stoyanova, R.; Zhecheva, E. *Chem. Mater.* **1999**, *11*, 52.
(55) Matsumura, Y.; Wang, S.; Nakagawa, Y.; Yamaguchi, C. *Synth. Met.* **1997**, *85*, 1411.
(56) Zhecheva, E.; Stoyanova, R.; Jiménez-Mateos, J. M.; Alcántara, R.; Lavela, P.; Tirado, J. L. *Carbon* **2002**, *40*, 2301.
(57) Nowak, L.; Lezanska, M.; Rozwadowski, M.; Rozploch, F.; Marciniak, W. *Appl. Surf. Sci.* **2002**, *201*, 182.
(58) Menachem, C.; Wang, Y.; Flowers, J.; Peled, E.; Greenbaum, S. G. *J. Power Sources* **1998**, *76*, 180.
(59) Zhou, X.; Zhuang, L.; Lu, J. *J. Phys. Chem. B* **2003**, *107*, 7783.

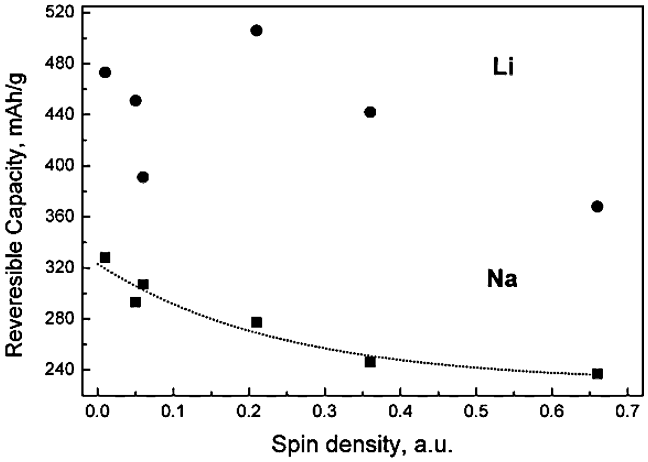

Figure 9. Specific capacity of microspherical carbon samples in sodium (square) and lithium (circle) cells vs spin density determined by EPR.

size graphene sheets, which are disordered and form the cavity walls. The variation in EPR signal intensity is related to the voltage hysteresis.[60] At 2 V of charge, the EPR intensity is higher than at 0 V because, although some lithium remains trapped in the carbon matrix, extraction of lithium clusters from cavities increases the EPR signal intensity because of microwave skin depth phenomena. In this line, previous studies showed the optical skin depth effect for Li intercalated disordered carbons by using in situ Raman spectroscopy.[61]

Taking into account all the results obtained, we derived an interesting experimental correlation between the spin density of the original localized radicals and the reversible capacity of carbon microbeads vs Na (Figure 9). The carbon microbeads characterized with a lower spin density display the higher reversible capacity vs Na. In the case of Li, the tendency is the same, but the correlation is less obvious when compared to Na. It then seems that the reaction of Li with the localized paramagnetic centers (dangling bonds) and terminal H is more reversible than the Na reaction. These EPR results are in line with the assignment of some excess Li capacity to edge sites.

3.5. ^{7}Li NMR. ^{7}Li NMR studies have been previously reported that investigate the intercalation of lithium into carbons.[62−67] Whereas metallic lithium exhibits a large, temperature-independent Knight shift at 260 ppm, fully lithiated graphite (LiC_6) exhibits a room-temperature ^{7}Li NMR signal centered at 40 ppm (small Knight shift), which is more broadened when the recording temperature decreases. The Knight shift is the shift of the resonance field due to hyperfine contact between conduction electrons and the nucleus. Graphitizable (soft) carbons obtained at about 700°C give a NMR signal at about 7 ppm that slightly shifts to more-positive parts per million values during cycling.[63] Other carbon modifications, which show higher capacities than LiC_6, exhibit more-complex NMR spectra. The exchange of lithium nuclei among lithium atoms at different sites is responsible for variations in the static NMR spectra recorded at several temperatures.[64] For nongraphitizable (hard) carbons, Guérin et al. observed three ^{7}Li static NMR Lorentzian signals at low temperatures that were assigned to covalently bonded, intercalated, and pseudometallic lithium species.[65] At room temperature, a complex exchange was observed between these signals. A fourth signal from the electrolyte was also observed. Dai et al. observed three main features in ^{7}Li MAS NMR spectra of fully lithiated hard carbon samples prepared from the pyrolysis of cotton cloth at 1000°C: a broad signal at ca. 50 ppm (ascribed to lithium intercalated between disordered graphene layers), a sharp line at 17 ppm (Li sites in hydrogen-containing regions), and a shoulder at about 0 ppm (surface film).[66] For vapor-grown carbon nanofibers, two narrow ^{7}Li MAS NMR signals placed at about 0 and 2−10 ppm were observed at room temperature that, after the carbon fibers were treated with refluxing nitric acid, were converted into a broadened single signal at about 0 ppm.[67]

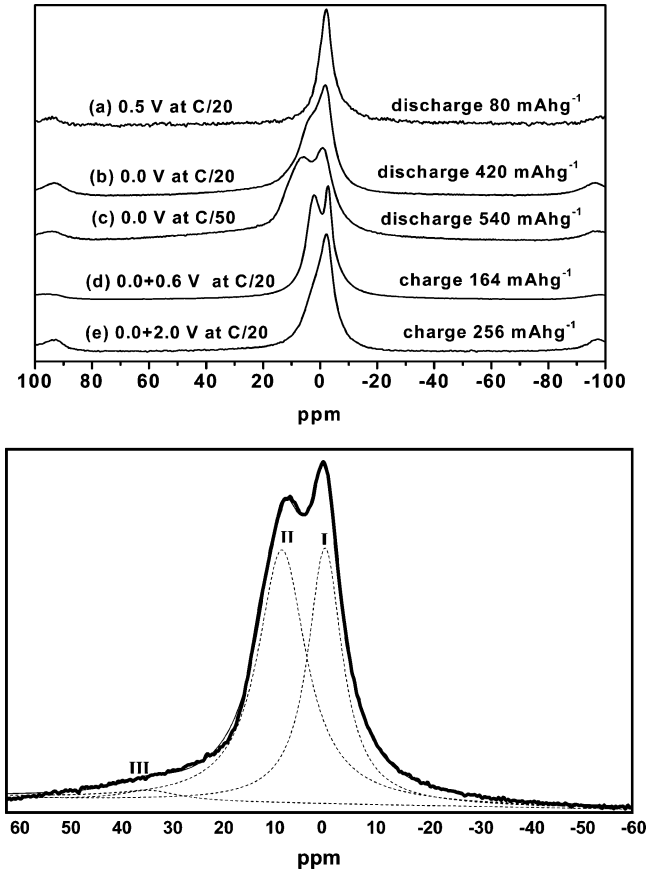

Figure 10. ^{7}Li NMR MAS spectra. Top: (a) first discharge to 0.5 V at a *C*/20 rate, (b) first discharge to 0.0 V at a *C*/20 rate, (c) first discharge to 0.0 V at a *C*/50 rate, (d) discharge to 0.0 V and charge to 0.6 V at a *C*/20 rate, and (e) discharge to 0.0 V and charge to 2.0 V at a *C*/20 rate. Bottom: detailed view of the experimental and simulated spectra of carbon discharged to 0.0 V at a *C*/50 rate. The electrodes were washed prior to NMR measurements.

(60) Wu, Y. P.; Wan, C. R.; Jiang, C. Y.; Fang, S. B.; Jiang, Y. Y. *Carbon* **1999**, *37*, 1901.
(61) Endo, M.; Kim, C.; Karai, T.; Fujino, T.; Matthews, M. J.; Brown, S. D. M.; Dresselhaus, D. S. *Synth. Met.* **1998**, *98*, 17.
(62) Tatsumi, K.; Kawamura, T.; Higuchi, S.; Hosotubo, T.; Nakajima, H.; Sawada, Y. *J. Power Sources* **1997**, *68*, 263.
(63) Tatsumi, K.; Akai, T.; Imamura, T.; Zaghib, K.; Iwashita, N.; Higuchi, S.; Sawada, Y. *J. Electrochem. Soc.* **1996**, *143*, 1923.
(64) Tatsumi, K.; Conard, J.; Nakahara, M.; Menu, S.; Lauginie, P.; Sawada, Y.; Ogumi, Z. *J. Power Sources* **1999**, *81*−*82*, 397.
(65) Guérin, K.; Ménétrier, M.; Février-Bouvier, A.; Flandrois, S.; Simon, B.; Biensan, Ph. *Solid State Ionics* **2000**, *127*, 187.
(66) Dai, Y.; Wang, Y.; Eshknazi, V.; Peled, E.; Greenbaum, S. G. *J. Electrochem. Soc.* **1998**, *145*, 1179.
(67) Ortiz, G.; Alcántara, R.; Lavela, P.; Tirado, J. L. *J. Electrochem. Soc.* **2005**, *152*, A1797.

Table 3. Fitting Results of ^{7}Li MAS NMR Spectra[a]

			signal I			signal II			signal III			signal IV			signal V		
discharge (D) or charge (C)	voltage (V)	rate	δ	W	C	δ	W	C	δ	W	C	δ	W	C	δ	W	C
D	0.5	*C*/20	−2.0	5.8	100												
D	0.0	*C*/20	−2.0	5.5	39	3.5	10.3	56	20.3	20.2	5						
D	0.0	*C*/50	−1.2	8.4	39	7.3	11.6	54	36.1	25.3	7						
D[b]	0.0	*C*/50	−1.3	1.9	8.0	12.7	7.3	2	36.0	28.3	23	4.9	67.4	61	−4.3	8.8	6
C	0.6	*C*/20	−2.8	3.1	31	2.2	6.4	69									
C	2.0	*C*/20	−2.4	5.4	52	1.9	9.6	42									

[a] δ = chemical shift (ppm); W = line width (ppm); C = contribution (%). [b] Unwashed electrode.

The ^{7}Li NMR MAS spectra of the lithiated microspherical carbon sample, after washing the electrodes with pure solvent, are shown in Figure 10. The main signal is located near 0 ppm, whereas spinning sidebands are also observed. The main signal was deconvoluted into several Lorentzian lines, and the results, obtained by using the DMFIT2004 program, are shown in Table 3.[68] For the electrode discharged down to 0.5 V at a *C*/20 rate, a single peak is observed at −2 ppm (peak I). For the electrode discharged down to 0.0 V at a *C*/20 rate, three peaks are found located at −2 ppm (peak I), +3.5 ppm (peak II), and +20.3 ppm (peak III). For the electrode discharged down to 0.0 V at a *C*/50 rate, three peaks are observed at −1.2 (peak I), +7.3 (peak II), and +36.1 ppm (peak III). The experimental and simulated spectra of this last electrode are shown in the bottom of Figure 10. It is worthy to note that in the time scale of the NMR experiments recorded at room temperature, exchange between different lithium sites is expected and an observed single peak may represent the mean situation between several peaks. The narrow peak I is ascribed to ionic lithium mainly from the passivating layer and traces of electrolyte. The relative intensity of peak I is at a maximum at 0.5 V of the first discharge and at 2 V of the charge process. Peaks II and III are ascribed to lithium inserted in the carbon electrode. The position of signal II is shifted to higher values when the discharge capacity increases (Table 3), and this peak is then mainly ascribed to lithium intercalated into disordered carbon (i.e., between graphene layers and in the edges). Peak III is broadened, exhibits low intensity (5−7% contribution), and corresponds to lithium with less ionic character formed at 0 V, mainly placed in cavities and adsorbed in the surface of graphene layers. Peak III is shifted to lower fields and its contribution is enhanced when the discharge is carried out at lower rate, which is probably indicative of the slower accessibility of lithium to these sites as compared to sites I and II. After complete discharge down to 0.0 V and then charge up to 0.5 or 2.0 V, peak III is not observed, whereas peaks I and II are still visible. This behavior indicates that some lithium atoms represented by peak II remain irreversibly trapped in the carbon electrode. This is in line with the EPR results shown above. The spectrum of the unwashed discharged electrode is shown in Figure 11. Two new signals are observed at +4 (signal number IV) and −5 (signal V) ppm, which are ascribed to electrolyte and lithium salts, respectively. The relative intensity of signal III is much higher for the unwashed electrode, which is in good agreement with previous studies.[65]

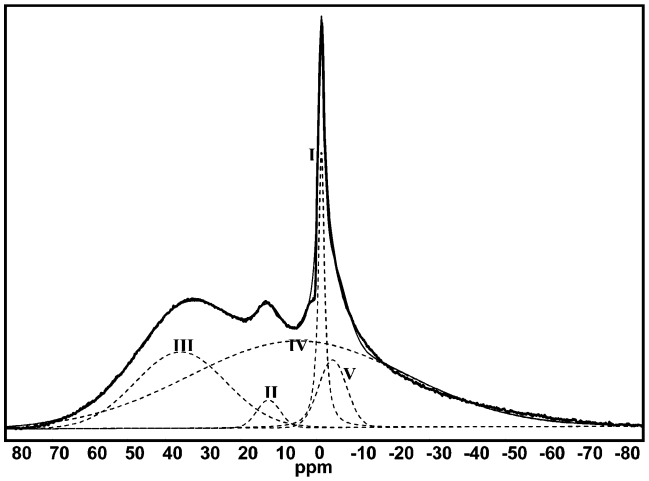

Figure 11. Detailed view of experimental and simulated ^{7}Li NMR MAS spectra of carbon microbeads discharged to 0.0 V at a *C*/50 rate. The electrode was unwashed.

Conclusions

Carbon microbeads have been prepared by the hydrothermal treatment of aqueous solutions of glucose. Further treatment of the carbonaceous microspherical particles with citric acid provides an adequate method for controlling the specific surface area and the occurrence of internal cavities and for optimizing the electrochemical behavior. Reversible capacities up to 550 mA h g^{-1} are achieved in lithium test cells. EPR and NMR spectra reveal that alkali metals are inserted in at least two sites of the nongraphitic carbon. The reaction of Li (and Na) with the localized paramagnetic centers (defects sites) that are found in the original carbon samples decrease the reversible specific capacity.

Acknowledgment. J.L.T., P.L., G.F.O., and R.A. acknowledge financial support from MEC (Contract MAT2005-00374 and Programa Ramón y Cajal). E.Z. and R.S. acknowledge the National Science Fund of Bulgaria for financial support (Contract Ch1304/2003).

CM060060P

(68) Massiot, D.; Fayon, F.; Capron, M.; King, I.; Calvé, S. L.; Alonso, B.; Durand, J. O.; Bujoli, B.; Gan, Z.; Hoatson, G. *Magn. Reson. Chem.* **2002**, *40*, 70.